A&A 442, 125–136 (2005)
DOI: 10.1051/0004-6361:20053168

Astronomy & Astrophysics

The evolution of early-type galaxies at $z \sim 1$ from the K20 survey⋆,⋆⋆

S. di Serego Alighieri[1], J. Vernet[1,⋆⋆⋆], A. Cimatti[1], B. Lanzoni[2], P. Cassata[3], L. Ciotti[4], E. Daddi[5], M. Mignoli[2], E. Pignatelli[6], L. Pozzetti[2], A. Renzini[7], A. Rettura[7,8], and G. Zamorani[2]

[1] INAF – Osservatorio Astrofisico di Arcetri, Largo E. Fermi 5, 50125 Firenze, Italy
e-mail: sperello@arcetri.astro.it
[2] INAF – Osservatorio Astronomico di Bologna, via Ranzani 1, 40127 Bologna, Italy
[3] Dipartimento di Astronomia, Università di Padova, Vicolo Osservatorio 2, 35122 Padova, Italy
[4] Dipartimento di Astronomia, Università di Bologna, via Ranzani 1, 40127 Bologna, Italy
[5] NOAO, 950 North Cherry Avenue, PO Box 26732, Tucson, AZ 85726, USA
[6] INAF – Osservatorio Astronomico di Padova, Vicolo Osservatorio 2, 35122 Padova, Italy
[7] European Southern Observatory, Karl-Schwarzschild-Str. 2, 85748 Garching bei München, Germany
[8] Université Paris-Sud 11, 15 rue Georges Clemenceau, 91405 Orsay, France

Received 31 March 2005 / Accepted 20 June 2005

ABSTRACT

We have performed VLT spectroscopy of an almost complete sample of 18 early-type galaxies with $0.88 \leq z \leq 1.3$ plus two at $z = 0.67$, selected from the K20 survey, and derived the velocity dispersion for 15+2 of them. By combining these data with HST and VLT images, we study the Fundamental Plane (FP), the Faber–Jackson and the Kormendy relations at $z \sim 1$. Compared with the local one, the FP at $z \sim 1$ has a remarkably small scatter, and shows both an offset and a rotation, which we interpret in terms of evolution of the mass-to-light ratio, and possibly of the size. We give evidence that the evolution rate depends on galaxy mass, being faster for less massive galaxies. We discuss the possible factors driving the evolution of spheroids and compare our results with the predictions of the hierachical models of galaxy formation.

Key words. galaxies: evolution – galaxies: elliptical and lenticular, cD – galaxies: kinematics and dynamics.

1. Introduction

The K20 survey (Cimatti et al. 2002c) with its selection in the near infrared and its very high spectroscopic redshift completeness (92%) provides an unprecedented tool for studying the history of galaxy mass assembly in the Universe, and in particular the formation of massive galaxies. In the currently popular ΛCDM scenario, massive galaxies are the product of rather recent hierarchical merging of pre-existing disk galaxies taking place largely at $z < 1.5$ and with moderate star formation rates (e.g. Kauffmann et al. 1993; and Cole et al. 2000). Therefore in such a hierachical merging scenario, fully assembled massive galaxies with $\mathcal{M} \geq 10^{11}\mathcal{M}_{\odot}$ and with evolved stellar populations should be very rare at $z \geq 1$. The alternative possibility is that massive systems formed at much higher redshifts (e.g. $z \geq 3$), through a short and intense period of star formation, followed by passive evolution of the stellar population. Such a possibility is supported by the properties of local and intermediate redshift spheroids (Renzini 1999), and by the existence of old and passive galaxies at $z \sim 1 \div 2$ (e.g. Cimatti et al. 2002a, 2004; McCarthy et al. 2004; Saracco et al. 2005). The controversy can then be solved by finding a number of evolved massive galaxies at $z \geq 1$. The problem so far has been the reliable determination of the mass, since the stellar masses estimated using the mass to infrared luminosity ratio or the fit to the multicolor spectral energy distribution are model dependent (IMF) and subject to various degeneracies (age – metallicity – extinction).

The advent of 8–10 m class telescopes has allowed dynamical masses to be estimated more reliably by kinematic studies of galaxies at $z \sim 1$. Various groups (e.g. van Dokkum & Stanford 2003; Treu et al. 2005b; Holden et al. 2005; Gebhardt et al. 2003; van der Wel et al. 2005, and references therein) have conducted kinematic studies of early-type galaxies, selected by optical morphology, both in the cluster and in the field environment up to $z \sim 1.3$. They have used the Fundamental Plane

⋆ Based on observations collected at the European Southern Observatory, Chile (ESO Programme 70.A-0548), and on observations with the NASA/ESA *Hubble Space Telescope*, obtained at the Space Telescope Science Institute, which is operated by AURA, Inc., under NASA contract NAS 5–26555.

⋆⋆ Figures 2 and 3 are only available in electronic form at http://www.edpsciences.org

⋆⋆⋆ *Present address*: ESO, Karl-Schwarzschild-Str. 2, 85748 Garching bei München, Germany.

(FP, Djorgovski & Davis 1987; and Dressler et al. 1987) to analyse the evolution of the $\mathcal{M}/L$ ratio, generally finding that the most massive spheroids must have formed at rather high redshift ($z \sim 3$). In order to understand the formation and evolution of early-type galaxies over a broader mass range it is necessary to extend these studies with different selection criteria and better completeness.

We address this problem by making spectroscopic observations of a sample of high redshift galaxies selected from the K20 survey, and by exploiting the large collecting area of the ESO Very Large Telescope (VLT), enhanced by the exceptionally good red sensitivity of FORS2 on the VLT. The selection of the K20 survey, being in the K_s band, which approximately corresponds to the rest frame J-band at the redshift of our sample, is much more sensitive to the stellar mass of the galaxy and much less dependent on the possible presence of star forming activity than the usual selection in the observed optical bands. Therefore it is suited to study the evolution of massive galaxies in a less biased way. Furthermore the spectroscopic classification of the K20 survey assigns a galaxy to the early-type class based on the presence of old stars, definitely a much more stable property than morphology and therefore less likely to exclude possible progenitors of today's spheroidal galaxies. In fact the only progenitors that we might miss are those where the clear spectroscopic signature of old stars would be overwhelmed by a major starburst, involving a considerable fraction of the galaxy mass. Our sample should therefore be less affected by the so called "progenitor bias" (e.g. van Dokkum & Franx 2001). Finally, the fact that the K20 survey and our study cover two independent fields, well separated in the sky, helps in reducing the effects of cosmic variance.

We describe here the results of our kinematic study on the early-type galaxies of the sample selected from the K20 survey, while a parallel paper (Vernet et al., in preparation) reports on those for disk galaxies. We assume a flat Universe with $\Omega_m = 0.3$, $\Omega_\Lambda = 0.7$, and $H_0 = 70$ km s^{-1} Mpc^{-1}, and we use magnitudes based on the Vega system.

2. Sample selection and observations

The galaxies to be observed have been selected from the K20 survey, which contains 545 objects selected in the K_s band, with $K_s < 20.0$, in two areas of the sky, the CDFS and 0055−269 fields covering 32.2 and 19.8 arcmin^2, respectively. We have selected galaxies with spectroscopic redshift between 0.88 and 1.3 and with early-type spectra, i.e. classified as class 1.0 (early-type galaxy without emission lines) and class 1.5 (early-type galaxy with emission lines) in the original K20 classification, based on a visual inspection of the spectra (Cimatti et al. 2002c). The limits of the redshift range, particularly the lower one, were set by the need of covering with a single spectroscopic setting the rest-frame wavelength interval between 3700 Å and 4500 Å, which contains the most useful absorption lines for the measurement of the velocity dispersion and the [OII]3727 emission line doublet.

Of the 14 and 10 galaxies selected with our criteria in the CDFS and 0055–269 fields respectively, we have observed 9 and 9 objects (see Table 1), i.e. 75%. The remaining objects have been excluded for purely practical reasons, i.e. they were either outside of the mask prepared for multi-object spectroscopy or their position was conflicting with that of other objects included in the mask. A better completeness has been achieved on the 0055−269 field because this, being smaller, is easier to cover with a single FORS2 mask. The result of our good completeness is that the observed galaxies span across the whole range of luminosities available for K20 early-type galaxies and give an unbiased view of the properties of early-type galaxies in the selected redshift and magnitude ranges. In order to check the properties of galaxies at lower redshift, we have included in the observed sample two galaxies at $z = 0.67$, one for each field. Recently a more quantitative classification of the K20 spectra has become available (Mignoli et al. 2005), with some differences with respect to the original visual classification. The only practical effect on our sample is that the galaxy identified as CDFS_00547 (which is class 1.5 in Cimatti et al. 2002c), with the recent reclassification would have been excluded from the sample, since it is not classified as an early-type galaxy, because its 4000 Å break is too small, although the spectral energy distribution is red (Mignoli et al. 2005). Of the 20 observed galaxies (see Table 1) 11 qualify as extremely red objects (ERO), according to the $R-K_s > 5.0$ definition (Elston et al. 1988), a confirmation of the power of this colour selection in identifying evolved galaxies at intermediate redshift.

The selected redshift range excludes the two peaks in the redshift distribution around $z \sim 0.67$ and $z \sim 0.74$ in the K20 survey (Cimatti et al. 2002b). Therefore our sample is most likely made of field galaxies, except for the two galaxies at $z = 0.67$, outside our main redshift range, which probably belong to the structures present at that redshift in both fields. The observed sample of galaxies is listed in Table 1. The reader is referred to the recent release of the K20 survey[1] for the object identification and for additional information on the individual galaxies.

The spectroscopic observations to obtain the velocity dispersion have been performed between 31 October and 2 November 2002 with FORS2 on UT4 of the ESO VLT at Paranal. We have used the grism 600z with slits 1.0 arcsec wide, which gives a resolution $\lambda/\Delta\lambda = 1400$ and covers the wavelength range 7400–10 700 Å. The rest–frame wavelength range for each individual galaxy, although varying according to its redshift and its position in the field, includes always the H and K [CaII] lines and the G band, except for one of the two lower redshift galaxies (q0055_00169), for which the spectrum starts around 4000 Å. We used two multi-object masks, one for each field. The exposure time was 7.5 and 6.0 h, and the average seeing was 0.7 and 0.625 arcsec for the CDFS and 0055–269 field respectively. For calibration we have observed the spectrophotometric standard stars Hiltner 600 and HD 49798.

For the morphological and photometric analysis we have used the HST+ACS 5 epochs mosaicked stacks $F850LP$ images from the Great Observatories Origin Deep Survey

[1] See `http://www.arcetri.astro.it/~k20/spe_release_dec04/index.html`

Table 1. The sample of observed early-type galaxies from the K20 survey.

K20 name	z	R	$R-K_s$	n	K_V	R_e kpc	$\langle\mu^B\rangle_e$ mag/arcsec^2	σ km s^{-1}	EW[OII] Å	M_B	$\log \frac{M_{K_V}}{M_\odot}$
CDFS_00060	1.188	24.89	5.56								
CDFS_00369	0.8930	23.30	4.14	1.85 ± 0.39	7.37 ± 0.18	0.84 ± 0.05	17.78 ± 0.15	119 ± 21	9.0 ± 1.1	–20.41	10.31 ± 0.15
CDFS_00467	0.8956	22.90	4.63	3.45 ± 0.39	5.72 ± 0.25	1.52 ± 0.10	18.40 ± 0.15	140 ± 18	4.3 ± 0.8	–21.09	10.58 ± 0.11
CDFS_00468	1.019	24.86	5.03								
CDFS_00532	1.2115	23.92	5.22	2.04 ± 0.33	6.82 ± 0.20	1.41 ± 0.10	17.43 ± 0.16	260 ± 30	2.5 ± 0.5	–21.89	11.16 ± 0.10
CDFS_00547	1.2243	23.68	5.07	1.90 ± 0.31	7.50 ± 0.14	0.74 ± 0.04	16.15 ± 0.14	256 ± 28	2.3 ± 0.4	–21.76	10.93 ± 0.10
CDFS_00571	0.9551	22.33	4.79	5.00 ± 0.15	3.83 ± 0.02	6.81 ± 0.48	20.65 ± 0.16	182 ± 21	3.7 ± 0.5	–22.08	11.23 ± 0.10
CDFS_00590	1.2235	24.35	5.28	4.98 ± 0.25	4.03 ± 0.12	4.09 ± 0.52	20.54 ± 0.29	119 ± 49	4.1 ± 1.1	–21.09	10.68 ± 0.36
CDFS_00633	1.0963	22.43	5.49	4.78 ± 0.21	4.00 ± 0.12	6.65 ± 0.12	19.97 ± 0.05	260 ± 23	<1.4	–22.71	11.55 ± 0.08
CDFS_00354	0.6672	22.01	4.07	3.58 ± 0.28	5.20 ± 0.20	3.08 ± 0.12	20.39 ± 0.09	99 ± 19	$2.6 \pm 0.6^*$	–20.61	10.52 ± 0.17
q0055_00028	1.0524	24.19	5.09	0.8 ± 0.8	7.17 ± 0.48	1.17 ± 0.65	18.08 ± 1.22	227 ± 30	<3.6	–20.82	10.99 ± 0.26
q0055_00068	1.1043	23.53	5.18	4.3 ± 1.0	4.55 ± 0.73	3.60 ± 1.00	19.75 ± 0.61	84 ± 31	2.3 ± 0.7	–21.60	10.37 ± 0.34
q0055_00114	0.8891	23.48	4.33	2.0 ± 2.0	6.71 ± 1.78	2.43 ± 0.74	19.99 ± 0.66	52 ± 22	<2.1	–20.50	9.98 ± 0.38
q0055_00123	0.9270	22.96	4.84	3.8 ± 1.0	5.69 ± 0.67	1.23 ± 0.40	17.62 ± 0.71	186 ± 19	1.6 ± 0.5	–21.39	10.74 ± 0.16
q0055_00247	0.931	24.43	4.54						<2.8		
q0055_00295	1.1680	23.75	5.59	4.8 ± 0.3	4.35 ± 0.20	2.67 ± 0.70	18.93 ± 0.57	170 ± 28	<1.4	–21.77	10.85 ± 0.18
q0055_00318	0.8962	23.87	5.07	4.5 ± 1.1	5.17 ± 0.70	1.26 ± 0.57	18.87 ± 0.99	105 ± 30	$<0.8^*$	–20.20	10.21 ± 0.31
q0055_00331	0.8980	22.95	5.09	4.9 ± 0.3	4.15 ± 0.19	3.83 ± 0.77	20.08 ± 0.44	216 ± 46	$<0.8^*$	–21.40	11.18 ± 0.19
q0055_00338	0.9324	23.12	4.96	2.8 ± 0.6	5.93 ± 0.50	2.41 ± 0.43	19.23 ± 0.39	113 ± 19	<2.5	–21.24	10.59 ± 0.16
q0055_00169	0.6699	22.70	4.23	1.3 ± 0.8	7.15 ± 0.62	1.64 ± 0.36	19.50 ± 0.47	90 ± 19	$<0.9^*$	–20.14	10.32 ± 0.20

* For [OIII]5007.

(GOODS, Giavalisco et al. 2004) and images from the ESO Imaging Survey (EIS, NTT+SUSI2 U, B, V, R and NTT+SOFI J, K_s) for the CDFS field, and images obtained with the NTT+SUSI2 (U, B, V, I), the NTT+SOFI (J, K_s) and the VLT+FORS1 (R, z) for the 0055−269 field.

3. Data analysis

3.1. Morphology

In order to obtain the effective radius R_e, we have fitted a Sérsic profile ($\log I(R) \propto -R^{1/n}$, Sérsic 1968) using GIM2D, a fitting algorithm for parametric two-dimensional models of surface brightness distribution (Simard et al. 1998). GIM2D performs a profile fit by deconvolving the data with the point spread function. We model PSFs with analytic functions from visually selected stars in the surrounding ($30'' \times 30''$) region of each galaxy. We model a different PSF for each region in order to take account of PSF variations with the position in the field. A 2D radial Gaussian function has been fitted simultaneously on tens of selected stars around the galaxies of our sample and outputs have been stacked together to result into a single PSF image for each region. A more detailed description of our approach in modellig GOODS/ACS galaxy morphologies in the $1.0 < z < 1.5$ range will be given in Rettura et al. (2005, in preparation).

The results of the bidimensional fit is the semimajor axis a_e of the projected elliptical isophote containing half of the total light, the axis ratio b/a and the Sérsic index n, which we have left as free parameters. The effective radius is computed from $R_e = a_e\sqrt{b/a}$ and is given in Table 1.

Magnitudes have been measured on the ground–based images using the SExtractor (Bertin & Arnouts 1996) BEST estimator. The average surface brightness within the effective radius (in mag/arcsec^2) is obtained from the absolute magnitude M: $\langle\mu\rangle_e = M + 5\log R_e + 38.567$, with R_e in kiloparsec.

In order to obtain the morphological parameters in the rest frame B band we have used the HST+ACS images taken with the *F850LP* filter and the VLT+FORS1 images taken with the Gunn z filter, since these are very close to the B band at the redshift of our galaxies. In any case a small K-correction has been applied following the prescriptions of Hogg et al. (2002) and Blanton et al. (2003) and using the excellent information which we have on the spectral energy distribution. The surface brightness has been corrected for the cosmological $(1+z)^4$ dimming. We have also corrected for the small Galactic extinction as obtained from Schlegel et al. (1998).

For the 0055–269 field we lack HST images, so we have to rely on very good quality VLT+FORS1 images (seeing 0.62 arcsec). Obviously the quality of the parameters obtained is worse than for those on the CDFS field. In order to check that the results are still acceptable and that the ground-based parameters are not biased, we have repeated the morphological analysis of the CDFS galaxies on a VLT+FORS1 image equivalent to that used for the 0055–269 field and found that the parameters obtained are consistent with those based on the HST+ACS images, although with larger errors (see Fig. 1).

In order to check our consistency with the results obtained by others fitting the de Vaucouleurs law, we have repeated our fits by fixing the Sérsic index to 4, obtaining sizes which are within 40% of those obtained with a variable index, some bigger, some smaller, but without a noticeable dependence on the n

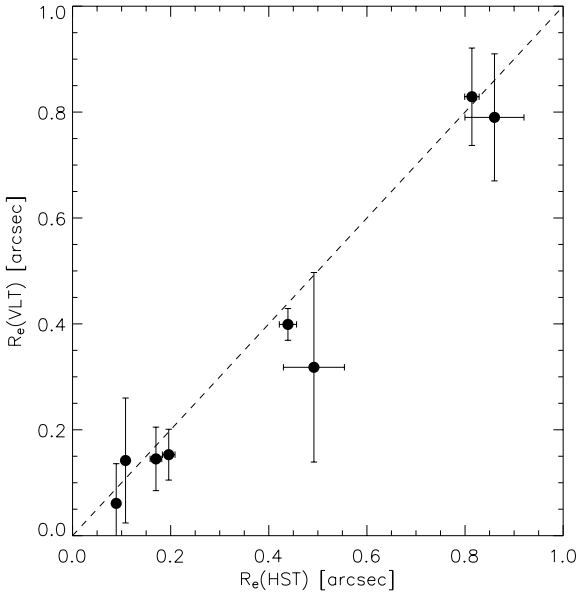

Fig. 1. Comparison of effective radii obtained for the CDFS field on the HST+ACS image and on the VLT+FORS1 one.

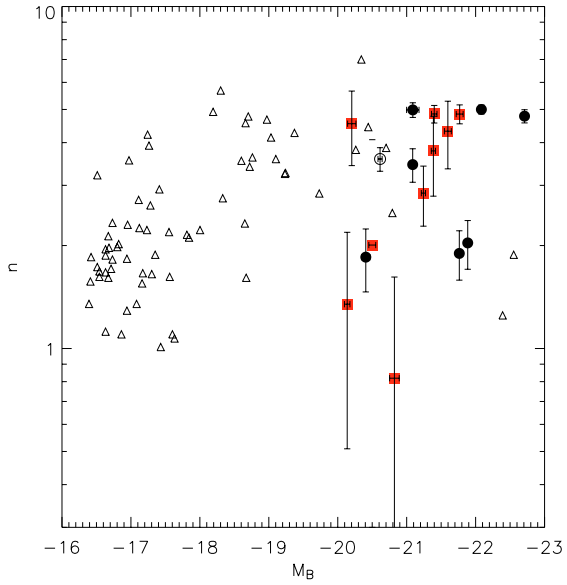

Fig. 4. The correlation of the Sérsic index with the luminosity. Triangles are the Coma cluster data of Gutiérrez et al. (2004), circles and squares are our $z \sim 1$ galaxies in the CDFS and 0055 − 269 fields respectively and empty symbols are for galaxies with $z < 0.88$, while filled ones are for our redshift range $0.88 < z < 1.3$.

value. The difference of the mean sizes derived with the two different fits is less than 5%.

3.2. Spectroscopy

The spectra have been reduced using the IRAF software package in the usual way, including atmospheric extinction correction and flux calibration. For each galaxy we have extracted a one-dimensional spectrum by coadding a section centred on the nucleus and one arcsecond long along the slit. This results in a spectral aperture of 1×1 arcsec^2. The extracted spectra are shown in Fig. 2.

The most noisy – i.e. sky contaminated – sections of the spectra have been masked out and the velocity dispersions have been obtained with the *xcor* task in IRAF, which uses the cross correlation technique of Tonry & Davis (1979). The correlation has been performed with template spectra of stars from the STELIB library (Le Borgne et al. 2003), with spectral types ranging from F6 to K2, by matching their spectral resolution to that measured on our spectra. We have made tests with spectra of template stars artificially smoothed to a known velocity dispersion, and with realistic noise added. These tests confirm that the results are not biased and that the quoted errors are realistic. The measured velocity dispersion has been normalized to a circular aperture with a diameter of 1.19 h^{-1} kpc, equivalent to 3.4 arcsec at the distance of the Coma cluster, following the prescriptions of Jørgensen et al. (1995b), as commonly used in FP studies. The changes on the velocity dispersion produced by these normalization factors are in any case small, i.e. 6–7%. The normalized velocity dispersion is listed in Table 1, except for CDFS_00060, CDFS_00468 and q0055_00247, for which we could not obtain a reliable value because of the low S/N ratio. These three galaxies are the faintest in the R band. The average redshift of the galaxies with measured velocity dispersion is $z = 1.071$ for the CDFS field and $z = 0.983$ for the 0055–269 one, excluding the two galaxies at $z = 0.67$.

Since we have noticed that several galaxies show a clear, although weak, [OII]3727 line emission, we have measured its rest–frame equivalent width (see Table 1). For the four galaxies, for which the [OII] line is outside the observed wavelength range, we have measured the [OIII]5007 line emission instead, as noted in the Table.

4. Results

4.1. Morphology

If one expects that all early-type galaxies should have a de Vaucouleurs profile, then the Sérsic indices that we obtain (see Table 1) appear rather small, and there are three galaxies in the CDFS and three in the 0055–269 field with $n < 2.5$. However also in the local Universe several early-type galaxies are found to have a small n (see Fig. 4). All the galaxies in our sample do have a prominent spheroidal component, although a disk is visible in a few of them (see Fig. 3), and all those in the CDFS field have been classified as E/S0 in the morphological analysis by Cassata et al. (2005), except for CDFS_00571, which is classified as Sa.

Moreover we find that the Sérsic index correlates with the B band absolute magnitude (see Fig. 4), as found at low redshift (e.g. Gutiérrez et al. 2004), but with a shift to brighter luminosities for the same values of n.

The distribution of the effective radii for our $z \sim 1$ galaxies is shifted towards smaller sizes with respect to low redshift samples (see Figs. 5 and 10). This could be due to a selection effect induced by the cosmological $(1 + z)^4$ dimming in surface brightness, in the sense that because of the dimming we

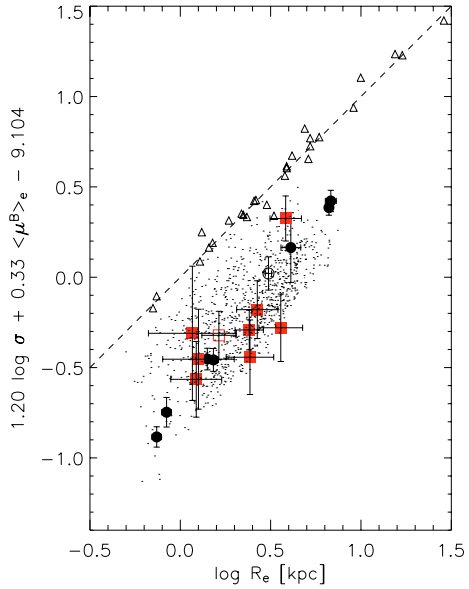

Fig. 5. The fundamental plane as obtained by Jørgensen et al. (1995a,b) for the Coma galaxies (triangles). Symbols are as in Fig. 4. The dashed line represents the best-fit plane to the Coma galaxies as seen edge-on. The small dots represent the GalICS model galaxies (see Sect. 5.2).

select higher surface brightness galaxies which tend to be more compact (see also Sect. 4.5).

Small sizes might also be due to the presence of an AGN in some of our galaxies, which could as well explain the large fraction of our objects showing [OII] emission, particularly in the CDFS field. Therefore we have checked the presence of our sample objects in the catalogue of X-ray sources presented by Alexander et al. (2003), obtained from the deep Chandra observations of the CDFS field by Giacconi et al. (2002). We found only one detection: galaxy CDFS_00467, which has a 0.5–8 keV X-ray flux of 2.2×10^{-16} erg cm^{-2} s^{-1}. For an unobscured type 1 AGN with an X-ray/optical ratio of 1, the corresponding observed magnitude would be $R \sim 26$, therefore contributing about 6% of the galaxy luminosity. However, since the source has a hardness ratio of ≈0.1, it is probably heavily obscured and much fainter in the R-band. Therefore its influence on the profile should be completely negligible.

4.2. The fundamental plane

The FP is a powerful tool to study the evolution of early-type galaxies. Because of its dependence on galaxy luminosity, it is sensitive to recent star formation episodes. Therefore the FP could be useful to study the influence of the environment on the galaxy evolution as, for example, star formation induced by merging.

We show in Fig. 5 the position of our $z \sim 1$ galaxies on the FP obtained by Jørgensen et al. (1996, hereafter JFK96) for the Coma galaxies at $z = 0.0248$ in the B-band. The FP at $z \sim 1$, compared to the local one, keeps a remarkably small scatter, particularly for the more accurate CDFS data, and shows a clear offset, as already noticed previously (e.g. Franx et al. 2000), and likely also a different tilt, suggesting that the evolution of

Table 2. The best fit parameters for the FP in the B-band.

Sample	Ref.	α	β	γ
Coma Cl.	0	1.20 ± 0.08	-0.83 ± 0.03	-0.17 ± 0.20
$0.88 < z < 1.3$	1	0.88 ± 0.16	-0.63 ± 0.04	0.46 ± 0.38

References. 0: JFK96; 1: this work.

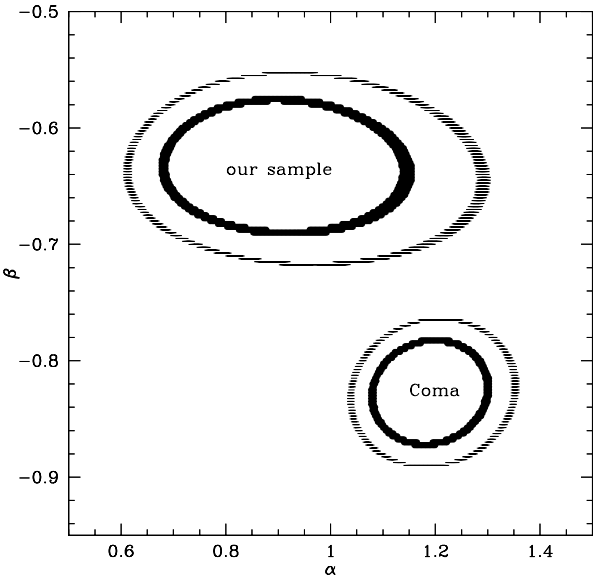

Fig. 6. 1-sigma (solid) and 90% (dashed) confidence regions of the joint distribution of the FP parameters α and β, for our data-set of $z \sim 1$ galaxies, and for the Coma cluster sample of JFK96.

early-type galaxies depends on their size and/or mass and/or stellar population.

In order to parametrize the offset and the rotation we have fitted a plane to the distribution of our data set, using the expression (e.g. JFK96):

$$\log R_e = \alpha \log \sigma + \beta \log \langle I \rangle_e + \gamma, \quad (1)$$

where $\langle I \rangle_e = L/2\pi R_e^2$, given the definition of the effective radius, is the average surface luminosity within R_e. We remind the reader that $\log \langle I \rangle_e = -0.4(\langle \mu \rangle_e - C)$, where $\langle I \rangle_e$ is in solar luminosities per square parsec, $\langle \mu \rangle_e$ is in magnitudes per square arcsecond and the constant C depends on the band, but not on the cosmology ($C_B = 26.982$, $C_K = 24.982$).

The rms scatter of the logR_e residuals from the best-fit FP is 0.11, while it becomes 0.17 when the Coma cluster parameters are assumed in the fit, as done in Fig. 5. The best-fitting values of α, β and γ have been derived by minimizing the sum of the square distances from the plane, weighted by the observational errors. They are listed in Table 2, together with those obtained for the Coma galaxies of JFK96 by means of the same procedure. The 90% confidence regions of the joint distribution of α and β, for our $z \sim 1$ galaxies, and for the Coma cluster sample of JFK96 (Fig. 6) are well separated, showing that no pair of (α, β) exists that simultaneously provides an acceptable fit to the two data-sets. As expected, such a result is almost completely due to ACS data, which have significantly smaller errors for both R_e and $\langle I \rangle_e$. However, we have verified that it

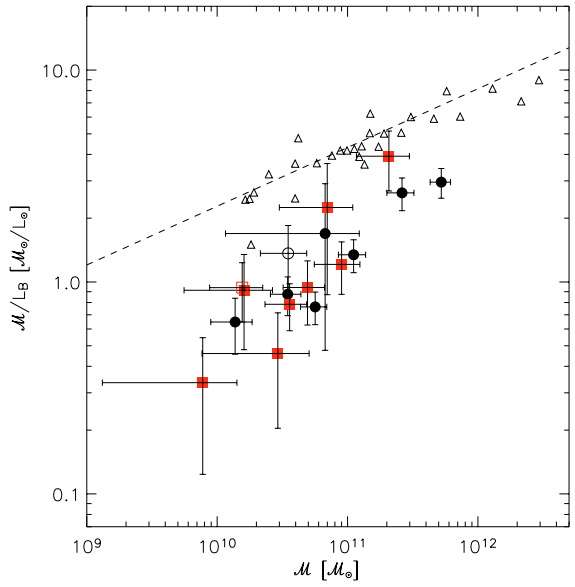

Fig. 7. Mass to light ratio vs. mass for our galaxies at $z \sim 1$ and for galaxies in Coma. Symbols are as in Fig. 4.

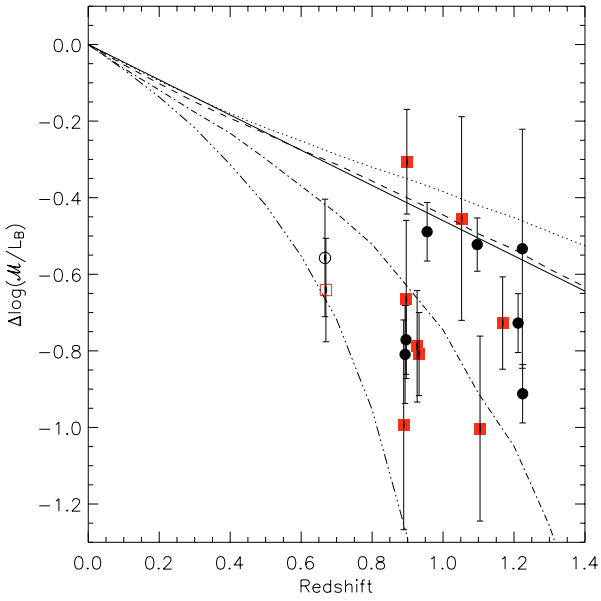

Fig. 8. Evolution of the mass to light ratio for our galaxies. Symbols are as in Fig. 4 and the continuous line is the linear fit obtained by van Dokkum & Stanford (2003) for the evolution of the mass to light ratio of cluster massive spheroids up to $z = 1.27$. The other lines are obtained with simple stellar population models using the Chabrier (2003) IMF with a formation redshift of 5.0, 3.0, 1.5 and 1.0 (*top to bottom*).

still holds if we use the values of R_e and $\langle I \rangle_e$ obtained from the de Vaucouleurs ($n = 4$) fit to the surface brightness profile. Thus our data show that at the 90% confidence level the FP rotates with redshift, even if larger samples are needed to better constrain its evolution.

In order to study the evolution of the $\mathcal{M}/L_B$ ratio in a way consistent with previous work, we assume that the dynamical mass of the galaxy is (Michard 1980):

$$\mathcal{M} = 5\frac{\sigma^2 R_e}{G}. \quad (2)$$

This assumption is equivalent to assuming $R^{1/4}$ homology among early-type galaxies. We relax this assumption in Sect. 4.4.

The evolution of the $\mathcal{M}/L_B$ ratio obtained in this way is shown in Figs. 7 and 8. The spheroidal galaxies at $z \sim 1$ have a brighter B-band luminosity for the same mass than low redshift galaxies by up to a factor of 8, particularly for the smaller mass galaxies. We note however that our sample goes to smaller masses than the Coma sample of Jørgensen et al. (1995a,b). The evolution in the $\mathcal{M}/L_B$ ratio is similar to that of the massive galaxies in clusters for ∼25% of our galaxies, while it is stronger for the rest of our sample (see Fig. 8).

Actually, as Treu et al. (2005a) and van der Wel et al. (2005), we find that the evolution is different for galaxies with different mass. If we fit a linear slope η to the evolution of the $\mathcal{M}/L_B$ ratio ($\Delta\log(\mathcal{M}/L_B) = \eta z$), then we obtain $\eta = -0.59 \pm 0.03$ for our 8 galaxies with $\mathcal{M} > 5\times10^{10}\ \mathcal{M}_\odot$ and $\eta = -0.86 \pm 0.05$ for our 9 galaxies with $\mathcal{M} < 5 \times 10^{10}\ \mathcal{M}_\odot$. These two slopes are significantly different, showing that the evolution depends on the galaxy mass (see also Sect. 5.1). The slope for the more massive galaxies is close to the value $\eta = -0.46 \pm 0.04$, obtained by van Dokkum & Stanford (2003) for cluster massive galaxies ($\mathcal{M} > 10^{11}\ \mathcal{M}_\odot$). In fact we obtain $\eta = -0.52 \pm 0.04$ for our 4 most massive galaxies ($\mathcal{M} > 10^{11}\ \mathcal{M}_\odot$).

Since our sample is selected in the K_s band (approximately rest-frame J-band), the evolution of the $\mathcal{M}/L_B$ ratio can hardly be due to selection effects, as could be the case if selection were in the observed optical bands, which for $z \sim 1$ are very sensitive to star formation.

4.3. Other scaling relations

Figure 9 shows the relation between the velocity dispersion and the absolute magnitude in the B band – the so-called Faber-Jackson relation (Faber & Jackson 1976). Here the trends are less clear than with the FP, also because even the low redshift objects show a large scatter. However $z \sim 1$ galaxies appear to be brighter than their $z = 0$ counterparts with the same velocity dispersion.

A clearer trend is shown by the purely morphological relation between the effective radius and the surface brightness, i.e. the Kormendy (1977) relation (Fig. 10). For a comparable size, $z \sim 1$ early-type galaxies are about 1–2 mag brighter in surface brightness than the low redshift ones. This could in part be due to a selection effect: in fact Fig. 10 shows the limit for $M_B < -20$, which roughly corresponds to our apparent magnitude limit of $R \lesssim 24.4$ for measuring the velocity dispersion. We also remark that the distribution of R_e at $z \sim 1$, although it partially overlaps the one for Coma, it is more concentrated to smaller sizes.

Using the K-band absolute magnitudes computed by Fontana et al. (2004) by modest extrapolations of Bruzual & Charlot (2003) models fitted to the spectral energy distribution of our galaxies, we have also obtained the Faber-Jackson relation in the K-band (Fig. 11). Most of our galaxies are

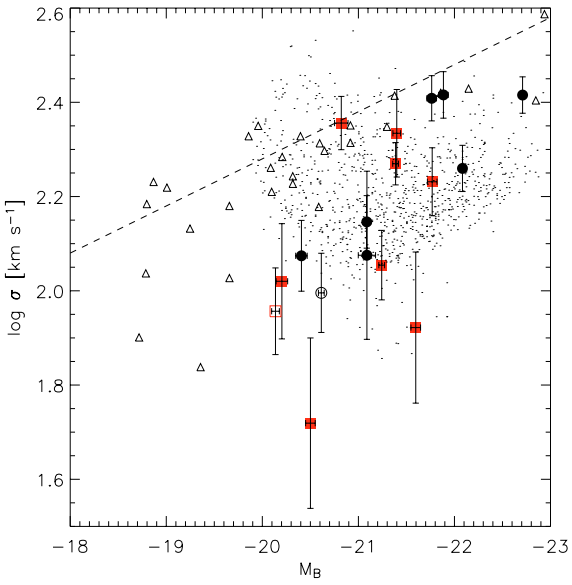

Fig. 9. The Faber-Jackson relation in the rest-frame B-band for our galaxies at $z \sim 1$ and for galaxies in Coma. Symbols are as in Fig. 4, small dots as in Fig. 5, the dashed line is the relation obtained at $z = 0$ by Forbes & Ponman (1999).

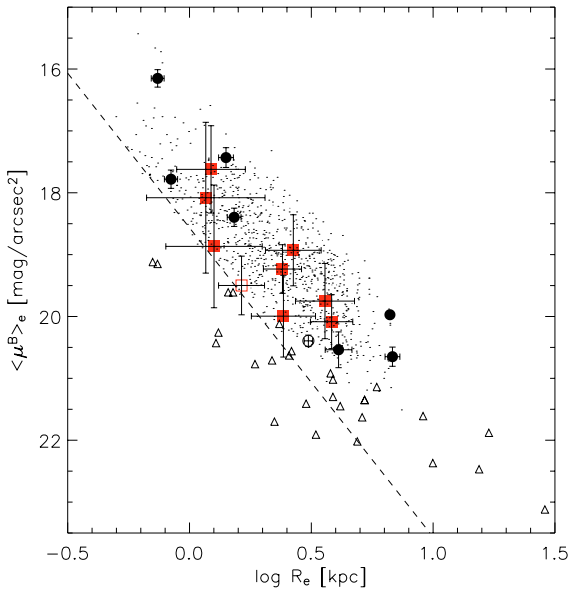

Fig. 10. The Kormendy relation in the rest-frame B-band for our galaxies at $z \sim 1$ and for galaxies in Coma. Symbols are as in Fig. 4 and small dots as in Fig. 5. The dashed line corresponds to $M_B = -20$.

brighter also in the K-band than their local counterparts with the same velocity dispersion, indicating some evolution of the $\mathcal{M}/L_K$ ratio.

4.4. Masses

We return to the determination of dynamical masses by relaxing the assumption of homology, which was used in Eq. (2). In fact we know that our galaxies are not homologous, since they have different Sérsic indices n, but seem to comply with a "weak homology", as n correlates with the luminosity (see

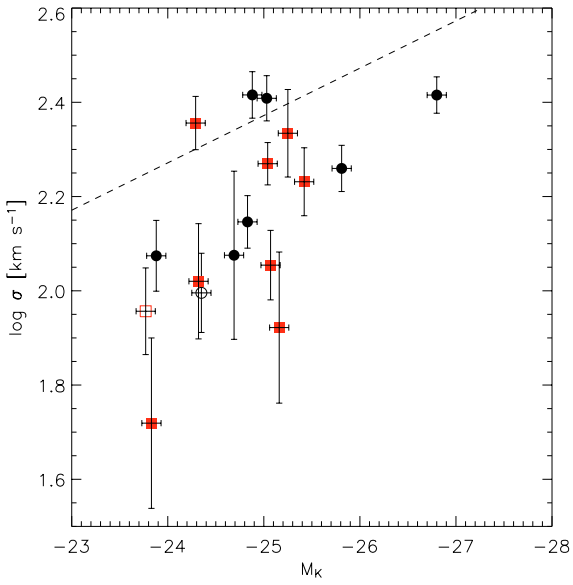

Fig. 11. The Faber-Jackson relation in the rest-frame K-band for our galaxies at $z \sim 1$. Symbols are as in Fig. 4, the dashed line is the local relation obtained for Coma cluster galaxies by Pahre et al. (1998).

Fig. 4). Bertin et al. (2002, BCD02 hereafter) have expressed the dynamical mass of a spheroidal galaxy in the form:

$$\mathcal{M}_{K_V} = K_V \frac{\sigma^2 R_e}{G}, \tag{3}$$

where K_V is a virial coefficient which takes into account the specific density distribution of both luminous and dark matter (DM), the specific star orbit distribution, and projection effects (see also Lanzoni & Ciotti 2003). By assuming spherical symmetry, global isotropy of the velocity dispersion tensor, and absence of DM, or a DM distribution which exactly parallels the stellar one, for a Sérsic profile, K_V only depends on the Sérsic index n and on the aperture within which the velocity dispersion σ has been measured. For instance, the commonly used factor 5 of Eq. (2) is appropriate for a de Vaucouleurs $R^{1/4}$ profile and for aperture radii of the order of $R_e/10$. An accurate fit of K_V for $1 \leq n \leq 10$ and small apertures ($R_e/8$) can be found in BCD02. We have recomputed it for the 1.7 kpc aperture to which we correct our velocity dispersion measurements. The resulting values of K_V and of $\mathcal{M}_{K_V}$ are listed in Table 1. We remark that this dynamical mass is larger by a factor of up to 1.55 than that estimated using Eq. (2). We emphasize the existence of an elliptical galaxy, i.e. CDFS_00633, at $z = 1.0963$ with red colors, a $R^{1/4}$ profile, no line emission, probably very low extinction, and a dynamical mass of 3.5×10^{11} $\mathcal{M}_\odot$.

We have compared our dynamical masses obtained with Eq. (3) with the stellar masses obtained by Fontana et al. (2004) for the K20 galaxies using their Best Fit model, where the spectrum best fitting the complete $UBVRIzJK_s$ multicolor photometry for Salpeter IMF is used. However since the Salpeter IMF is known to be inadequate (see e.g. Renzini 2005; and Bruzual & Charlot 2003) and all empirical determinations of the IMF indicate that its slope flattens below $\sim$0.5 $\mathcal{M}_\odot$ (Kroupa 2001; Gould et al. 1996; Zoccali et al. 2000), we have divided the stellar masses of Fontana et al. (2004) by a factor of 1.72, which

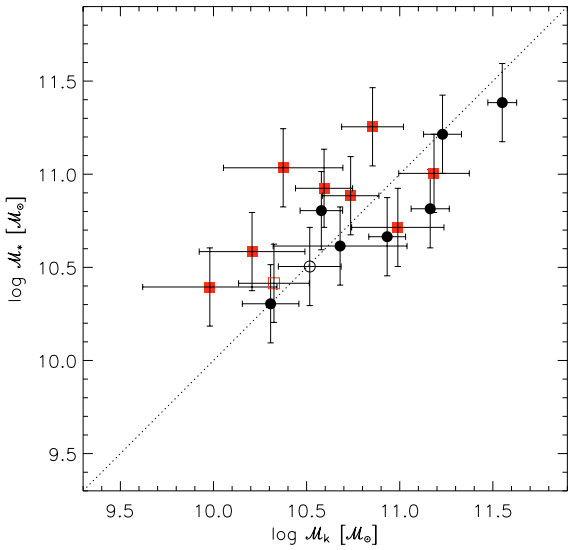

Fig. 12. The comparison of dynamical and stellar masses for our sample at $z \sim 1$. Symbols are as in Fig. 4.

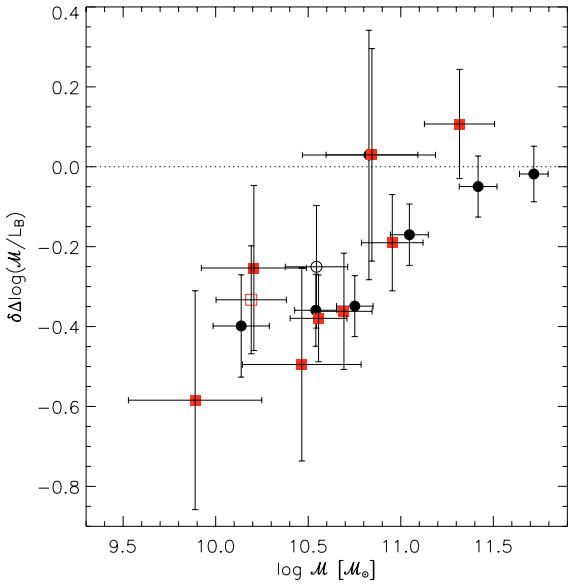

Fig. 13. The differential evolution of the $\mathcal{M}/L_B$ ratio for each individual galaxy of our sample with respect to that of old cluster massive galaxies at the same redshift (see text). Symbols are as in Fig. 4.

is the age-averaged correction for a Chabrier (2003) IMF. The comparison is shown in Fig. 12.

The agreement between dynamical and stellar masses is good for the high mass galaxies, but most of our lower mass galaxies have stellar masses larger than the dynamical ones, with the maximum difference reaching a factor of four. Similar results have been recently found for lower redshift galaxies by Drory et al. (2004), who however attribute the discrepancy to the limited reliability of the SDSS velocity dispersion measurements for low masses galaxies. We also remark that, given our large spectroscopic aperture (in units of R_e), in case of substantial rotational support, the adopted normalization of the observed velocity dispersion (Sect. 3.2) might be incorrect, and the dynamical masses of the stellar component underestimated (Riciputi et al. 2005). This might be the case particularly for the lower mass objects, that are also those showing a faster evolution in the $\mathcal{M}/L_B$ ratio (see Sect. 5.1 and Fig. 13).

4.5. Comparison with previous results

Van der Wel et al. (2005), who have also analysed the FP for galaxies in the CDFS, have two objects in common with us: their objects CDFS–18 and CDFS–19 are our CDFS_00633 and CDFS_00571 respectively. Our results are in reasonable agreement with theirs. More specifically, considering ours vs. their results for CDFS_00633 and for CDFS_00571, the R_e is 6.65 ± 0.12 vs. 4.17 ± 0.3 kpc and 6.81 ± 0.48 vs. 2.69 ± 0.2 kpc, the velocity dispersion is 260 ± 23 vs. 324 ± 32 km s^{-1} and 182 ± 21 vs. 229 ± 35 km s^{-1}, the K magnitude is 16.94 vs. 16.98 and 17.54 vs. 17.53, the $U - B$ color is 0.54 vs. 0.32 and 0.26 vs. −0.32, the derived dynamical mass in $10^{11} \mathcal{M}_\odot$ is 3.5 ± 0.7 vs. 5.1 ± 1.0 and 1.7 ± 0.4 vs. 1.7 ± 0.5 (we have used here the masses derived with Eq. (2), which is also assumed by van der Wel et al. 2005).

This comparison suggests that our effective radii are somewhat larger than theirs, particularly for CDFS_00571. Our velocity dispersions and dynamical masses are comparable to theirs. Surprisingly they have much bluer colors than us, particularly for CDFS_00571, for which their value seems too blue, and in fact it is not plotted in their Fig. 8.

With respect to the morphological parameters obtained for the K20 galaxies in the CDFS field by Cassata et al. (2005), we have refined those previous values on a much smaller sample of objects by interactive optimization of fits of individual galaxies, masking out nearby objects and adjusting the local sky level. In general Cassata et al. (2005) also find a decrease of the galaxy size with redshift, particularly for the elliptical galaxies.

Daddi et al. (2005) also have obtained morphological parameters for 7 luminous early-type galaxies with $1.4 < z < 2.5$ using Sérsic profile fits with GALFIT on very deep HST+ACS images. They obtain small effective radii, even slightly smaller than ours, and a wide range of Sérsic indices: $1 < n < 10$.

Finally, in comparing our relatively small sizes to the sizes obtained by others it is important to note that our spectroscopic galaxy type selection favours compact objects, while a morphological type selection, such as e.g. that of Treu et al. (2005a,b), favours brighter and therefore probably larger objects.

5. Discussion

5.1. Spheroid evolution

The observed offset of the $z \sim 1$ FP from the local one is the result of the evolution of one or more physical properties of spheroids. This could be either the $\mathcal{M}/L$ ratio, as in the classical analysis, or the size R_e, or a combination of these two. Some evolution in the luminosity is actually expected as constituent stars grow older, even in the most passive scenario (see the models in Fig. 8). However there is also evidence of size evolution both from our data and from others (see Sect. 4.1). It is however not clear what the exact relative weight is of these

two contributions to the evolution of spheroids, and how an individual object evolves in size.

The observed rotation of the FP implies that the evolution of spheroids is not the same for all of them, whatever the evolving parameter. Some have argued that the evolution could be mass dependent in the sense that lower mass galaxies evolve later than more massive ones (Fontana et al. 2004; Pozzetti et al. 2003). Very recently Treu et al. (2005a) and van der Wel et al. (2005) have analysed the results of kinematic studies of field early-type galaxies with $0.2 < z < 1.2$ in terms of a mass-dependent evolution. In Sect. 4.2 we have already shown that the $\mathcal{M}/L_B$ evolution of our early-type galaxies depends on their dynamical mass. This is clearer in Fig. 13, where the difference between the $\mathcal{M}/L_B$ evolution of our galaxies and the fit derived by van Dokkum & Stanford (2003) for the cluster massive galaxies ($\delta\Delta\log(\mathcal{M}/L_B) = \Delta\log(\mathcal{M}/L_B)+0.46\,z$) is plotted as a function of mass. The dependence of the differential $\mathcal{M}/L_B$ evolution on mass appears to have a threshold around $10^{11}\mathcal{M}_\odot$, in the sense that more massive galaxies evolve in a way similar to that of cluster massive galaxies, while less massive objects evolve progressively faster and their $\mathcal{M}/L_B$ ratio is lower than that of cluster massive galaxies by a factor of up to about 3 for galaxy masses of the order of $10^{10}\mathcal{M}_\odot$. We emphasize that the differential $\mathcal{M}/L_B$ evolution, clearly visible in Fig. 13 and in similar figures by Treu et al. (2005a) and by van der Wel et al. (2005), implies that the FP must rotate with redshift (Renzini & Ciotti 1993).

The differential $\mathcal{M}/L_B$ evolution which we observe is similar to the so-called "downsizing" (Cowie et al. 1996; see also Kodama et al. 2004; Treu et al. 2005a), i.e. the later and/or longer lasting formation of lower mass galaxies. The reason for such later evolution of less massive spheroids could be found in a change with mass of either their stellar populations (IMF, age, metallicity), or of some structural/dynamical parameter, such as the DM distribution, the density profile, the degree of anisotropy and the partial rotational support, or a combination of these. However the only structural/dynamical changes possible during the Universe lifetime are those induced by merging.

A testable hypothesis is that the lower mass-to-light ratio of the less massive galaxies is due to recent star formation or younger ages increasing their B-band luminosity. We have therefore looked at the dependence of $\delta\Delta\log(\mathcal{M}/L_B)$ on star formation indicators as the [OII] equivalent width and the rest-frame $U-B$ color. The dependence on the [OII] equivalent width (Fig. 14) does not show any correlation, indicating that the lower $\mathcal{M}/L_B$ ratio is not due to on-going star formation activity. This is actually consistent with the fact that our galaxies have been selected as having early-type spectra and that the detected [OII] line fluxes correspond to a rather low star formation rate, ranging between 0.10 and 0.18 $\mathcal{M}_\odot\ \mathrm{yr}^{-1}$, using the conversion of Kewley et al. (2004) and assuming no extinction. On the other hand a correlation exists between the differential evolution in $\mathcal{M}/L_B$ ratio and the $U-B$ color (Fig. 15), with galaxies with lower $\mathcal{M}/L_B$ ratio being bluer, indicating that indeed star formation activity has been proceeding until a rather recent past in the lower mass galaxies.

As anticipated in Sect. 4.4, the combined effect of substantial rotational support and large spectroscopic apertures in the low-mass galaxies (e.g., Davies et al. 1983) could produce a trend similar to differential evolution. In fact, aperture velocity dispersion of isotropic rotators, measured at or beyond R_e, can be significantly lower than the same quantity measured in the central region. Thus, the empirical correction of Jørgensen et al. (1995b; see Sect. 3.2), that has been locally determined from velocity dispersion profiles obtained through small spectroscopic apertures (where the effect of rotation is negligible), might not be appropriate in our case (large apertures) if rotation is important. Unfortunately, a quantitative estimate of such an effect is not easy; however, a detailed analysis of rotational and flattening effects on aperture velocity dispersion of axysimmetric galaxy models shows that the variation is of the

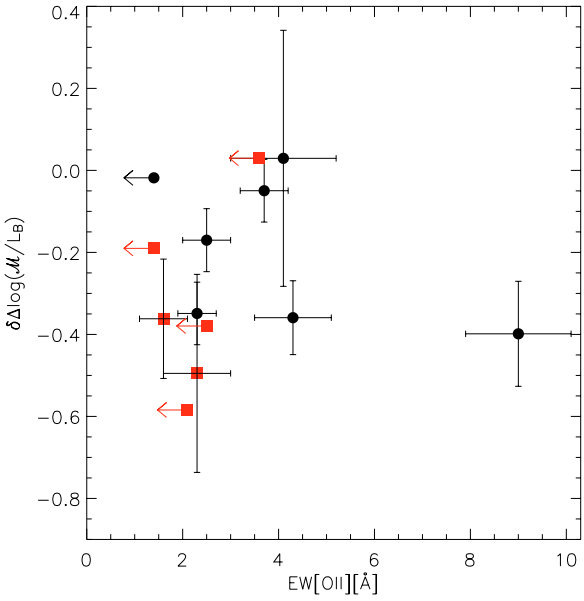

Fig. 14. The dependence of the differential evolution in $\mathcal{M}/L_B$ on the rest-frame equivalent width of the [OII]3727 emission line for our spheroidal galaxies at $z \sim 1$. Symbols are as in Fig. 4.

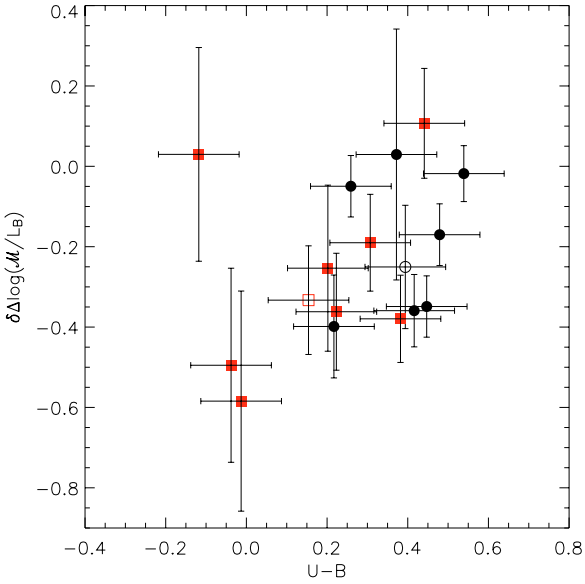

Fig. 15. The dependence of the differential evolution in $\mathcal{M}/L_B$ on the rest-frame $U-B$ color. Symbols are as in Fig. 4.

order of ≈30% for apertures of $\approx R_e$ (Riciputi et al. 2005; it increases up to ≈80% when the whole galaxy image is taken into account, as assumed by Bender et al. 1992), much less than our estimated differential evolution. Note however that the correction could be larger if a rotating disk is also present (see CDFS_00571 in Fig. 3). In order to check the importance of this effect on our data, we have looked for signs of rotation in the two-dimensional spectra of our galaxies with line emission. Unfortunately the emission lines are too faint and compact to show any signs of rotation at the S/N ratio of our spectra.

Data in Fig. 13 were obtained under the assumption of strong $R^{1/4}$ homology (Eq. (2)), and so it is natural to ask how the same figure is modified by adopting instead Eq. (3). In fact we know that our fainter galaxies have smaller Sérsic indices (see Fig. 4), and, since low n correspond to high values of K_V, this may reduce the predicted differential evolution. However the *maximum* effect due to non-homology is of the order of 55% (see Sect. 4.4), and therefore, as in the case of rotation, much smaller than the required factor of 3.

Of course, the two effects above could combine and reduce the amount of required intrinsic differential evolution, but it seems to be impossible to blame just systematic effects for the behavior of data in Fig. 13, for which younger mean ages for low mass galaxies probably have a major effect (Fig. 15).

5.2. Comparison with hierarchical models predictions

One of the currently open questions of observational cosmology is whether the observed evolution of early-type galaxies is consistent with the predictions of the hierarchical theories of galaxy formation. Our sample of early-type galaxies, being selected in the K band, which is particularly sensitive to galaxy mass, and being at the highest redshifts for which kinematic information has been obtained so far, is particularly well suited for this check.

If the early-type galaxies form by merging, as predicted by the hierarchical models, then we should see a different evolution in the cluster and in the field environment, where the merging probabilities can be different. We fail to observe such an effect, since our most massive field spheroids evolve at a rate indistinguishable from that of massive spheroids in clusters, and in the lower mass range there appear to exist early-type galaxies in clusters that evolve at a faster rate, comparable to that of our less massive field galaxies. Examples of this are our two galaxies at $z = 0.67$, which definitely evolve faster than cluster massive galaxies, although they are also likely in clusters. We note that also the two galaxies with $\mathcal{M} < 10^{11}\mathcal{M}_\odot$ in Fig. 6a of van Dokkum & Stanford (2003) and the two lowest mass E+A galaxies observed by van Dokkum et al. (1998) in a cluster at $z = 0.83$ appear to have a lower $\mathcal{M}/L$ ratio than the massive galaxies in the same cluster. We do not exclude that the evolution of spheroids may also depend on the environment, but to test this hypothesis it is necessary to study the FP on well selected and complete samples of *cluster* early-type galaxies, overcoming the obvious observational effect that usually prevents less luminous galaxies from finding empty slits in multi-object spectroscopic observations of high density cluster fields.

If, as predicted by some versions of the hierarchical merging model, the stellar populations of more massive galaxies are appreciably younger than those of smaller galaxies, the FP should become flatter with increasing redshift (e.g., Renzini 1999). This is contrary to the observed steepening of the FP, and suggests that, if spheroids form by merging, the building blocks of the most massive objects at $z \sim 1$ should have formed and assembled well before those constituting the lower mass galaxies at the same redshift.

To further check the ability of the hierarchical scenario in describing how galaxies form and evolve in the Universe, we have compared our results with the predictions of GalICS (Hatton et al. 2003), a hybrid (N-body and semi-analytic) hierarchical model of galaxy formation, that matches rather well the redshift distribution of the K20 survey (Blaizot et al. 2005). To perform a proper comparison with the observations, we have selected all field elliptical and S0 galaxies with $K_s < 20$ and $R < 24.4$ in 3 timesteps, corresponding to redshifts $z = 0.87, 1.01$ and 1.23. Although semi-analitic models are unable, by construction, to resolve the internal structure and dynamics of galaxies, spheroidal components in GalICs are approximated as Hernquist (1990) spheres, characterized by a half-mass radius r_h and a velocity dispersion at r_h (see Hatton et al. 2003, for details). We have therefore used the Hernquist model to correct these values and derive the corresponding effective radius R_e and the one-dimensional velocity dispersion within a $1.19\,h^{-1}$ kpc aperture, consistently with what done for the observations. The resulting values and the corresponding effective surface brightness have been used to build the simulated scaling relations, that are shown in Figs. 5, 9 and 10. The predicted FP appears to be similar to the observed one, even if its scatter is larger than observed. A good agreement is found for the Kormendy relation, while the discrepancies at the faint end of the Faber-Jackson relation suggest excessively large velocity dispersions and/or underestimated B-luminosities for simulated objects with $M_B \lesssim -21$. The model stellar masses, instead, are found to be in the correct range, between 10^{10} and $2 \times 10^{11}\mathcal{M}_\odot$. If one considers that the definition of morphological types in the model (based on the bulge-to-disc luminosity ratio in the B band) is different from the one adopted in the observations, and that structural and dynamical properties of galaxies can be only roughly described in this kind of modelling, the present comparison can be considered quite satisfactory. However, a major problem exists concerning the colours of simulated galaxies, which are too blue compared to the observations: for the selected GalICS sample, the rest-frame $B - K$ ranges between 1.9 and 4.6, with median at ∼3, while all observed galaxies have $B - K > 3.2$. In addition, excessively large dust extinctions are needed to obtain the reddest colours in the model galaxies. This is a well known, but still unsolved, problem common to all semi–analytic and hybrid models of this kind (see, e.g., Firth et al. 2002; Benson et al. 2002; Pozzetti et al. 2003; Somerville et al. 2004), suggesting that a re-examination of how star formation proceeds in galaxies is required, particularly at high redshift.

6. Conclusions

We have obtained photometric (total magnitudes in various bands), morphological (effective radius, average surface brightness within the effective radius, Sérsic index) and kinematic (velocity dispersion) parameters for an almost complete sample of 15 field early-type galaxies selected from the K20 survey in the redshift range $0.88 \leq z \leq 1.30$. Apart from completeness, our sample has the advantage of being selected in the K-band, of having the galaxy type assigned spectroscopically, and of covering two separate fields.

From these data we obtain the following results:

1. The distribution of effective radii is shifted towards smaller sizes compared to the local one.
2. Sérsic indices span a range between 0.5 and 4, and correlate with B-band luminosity.
3. The resulting FP in the rest-frame B-band at $z \sim 1$ is offset from, and steeper than, the local one, but keeps a remarkably small scatter.
4. Under the assumption of homology, and at fixed R_e, the evolution of the dynamical $\mathcal{M}/L_B$ ratio shows a dependence on galaxy mass: for our more massive objects, it is similar to that of *cluster massive galaxies*, while it is faster for the less massive ones, with a threshold around $10^{11}\mathcal{M}_\odot$.
5. For a given velocity dispersion or size some of the $z \sim 1$ galaxies are considerably brighter than local ones, both in the rest-frame B- and K-band.
6. Dynamical masses (properly obtained by taking into account the observed Sérsic index) are consistent with stellar masses (derived from model fits to the spectral energy distribution) in the high mass range, while they are smaller in the low mass range.
7. In about half of our $z \sim 1$ early-type galaxies we have detected [OII] line emission, corresponding to a low star formation rate ranging from 0.10 to 0.18 $\mathcal{M}_\odot\,\mathrm{yr}^{-1}$.

We give the following interpretation:

1. Spheroidals evolve in $\mathcal{M}/L$ ratio, and possibly also in size.
2. The rate of evolution over the last 2/3 of the Universe lifetime depends on the galaxy mass, low mass galaxies evolving faster.
3. A fraction of the detected differential evolution might be due to a stronger rotational support in low mass galaxies with respect to the high mass ones, and to the fact that observational data are routinely interpreted under the assumption of strong homology. However the correlation with galaxy color indicates that a significant fraction of the detected differential evolution is indeed intrinsic, i.e. due to more recent star formation episodes (the so-called "downsizing").
4. We fail to detect differences in the evolution with the environment, and the rotation of the FP goes in the opposite sense than predicted by the hierarchical merging models.
5. The GalICS hierarchical galaxy formation model is able to produce galaxies which are in the correct mass and size range and reproduce the various scaling relations, although with a larger scatter for the FP and with unrealistic colours and dust extinctions.

Since neither homology (constant K_V) nor the other extreme case of weak homology (constant mass-to-light ratio, BCD02) appear to be holding for our $z \sim 1$ spheroids, we are astonished that the FP keeps such a small scatter, while shifting and rotating as the Universe evolves, thus posing additional and more stringent challenges to our understanding of galaxy formation and evolution.

Acknowledgements. We are grateful to Julien Devriendt, George Djorgovski, Gianni Fasano, Alberto Franceschini and Tommaso Treu for helpful discussions. We thank Rino Bandiera, Jaron Kurk and Marco Scodeggio for useful software advice, Adriano Fontana for providing the stellar masses, and the referee for constructive comments. This research has made use of NASA's Astrophysics Data System and of the SIMBAD database, operated at CDS, Strasbourg, France.

References

Alexander, D. M., Bauer, F. E., Brandt, W. N., et al. 2003, AJ, 126, 539
Bender, R., Burstein, D., & Faber, S. M. 1992, ApJ, 399, 462
Benson, A. J., Ellis, R. S., & Menanteau, F. 2002, MNRAS, 336, 564
Bertin, E., & Arnouts, S. 1996, A&AS, 117, 393
Bertin, G., Ciotti, L., & Del Principe, M. 2002, A&A, 386, 149 (BCD02)
Blanton, M. R., Brinkmann, J., Csabai, I., et al. 2003, AJ, 125, 2348
Blaizot, J., Wadadekar, Y., Guiderdoni, B., et al. 2005, MNRAS, 360, 159
Bruzual, G., & Charlot, S. 2003, MNRAS, 344, 1000
Cassata, P., Cimatti, A., Franceschini, A., et al. 2005, MNRAS, 357, 903
Chabrier, G. 2003, PASP, 115, 763
Cimatti, A., Daddi, E., Mignoli, M., et al. 2002a, A&A, 381, L68
Cimatti, A., Pozzetti, L., Mignoli, M., et al. 2002b, A&A, 391, L1
Cimatti, A., Mignoli, M., Daddi, E., et al. 2002c, A&A, 392, 395
Cimatti, A., Daddi, E., Renzini, A., et al. 2004, Nature, 430, 184
Cole, S., Lacey, C. G., Baugh, C. M., & Frenk, C. S. 2000, MNRAS, 319, 168
Cowie, L. L., Songaila, A., Hu, E. M., & Cohen, J. G. 1996, AJ, 112, 839
Daddi, E., Renzini, A., Pirzkal, N., et al. 2005, ApJ, 626, 680
Davies, R. L., Efstathiou, G., Fall, S. M., Illingworth, G., & Schechter, P. L. 1983, ApJ, 266, 41
Djorgovski, S., & Davis, M. 1987, ApJ, 313, 59
Dressler, A., Lynden-Bell, D., Burnstein, D., et al. 1987, ApJ, 313, 42
Drory, N., Bender, R., & Hopp, U. 2004, ApJ, 616, L103
Elston, R., Rieke, G. H., & Rieke, M. J. 1988, ApJ, 331, L77
Faber, S. M., & Jackson, R. E. 1976, ApJ, 204, 668
Firth, A. E., Somerville, R. S., McMahon, R. G., et al. 2002, MNRAS, 332, 617
Fontana, A., Pozzetti, L., Donnarumma, I., et al. 2004, A&A, 424, 23
Forbes, D. A., & Ponman, T. J. 1999, MNRAS, 309, 623
Franx, M., van Dokkum, P. G., Kelson, D., Fabricant, D. G., & Illingworth, G. D. 2000, Phil. Trans. R. Soc. Land. A, 358, 2109
Gebhardt, K., Faber, S. M., Koo, D. C., et al. 2003, ApJ, 597, 239
Giacconi, R., Zirm, A., Wang, J., et al. 2002, ApJS, 139, 369
Giavalisco, M., Ferguson, H. C., Koekemoer, A. M., et al. 2004, ApJ, 600, L93
Gutiérrez, C. M., Trujillo, I., Aguerri, J. A. L., et al. 2004, ApJ, 602, 664
Gould, A., Bachall, J. N., & Flynn, C. 1996, ApJ, 465, 759

Hatton, S., Devriendt, J. E. G., Ninin, S., et al. 2003, MNRAS, 343, 75
Hernquist, L. 1990, ApJ, 356, 359
Hogg, D. W., Baldry, I. K., Blanton, M. R., & Eisenstein, D. J. 2002 [arXiv:astro-ph/0210394]
Holden, B. P., van der Wel, A., Franx, M., et al. 2005, ApJ, 620, L83
Jørgensen, I., Franx, M., & Kjærgaard, P. 1995a, MNRAS, 273, 1097
Jørgensen, I., Franx, M., & Kjærgaard, P. 1995b, MNRAS, 276, 1341
Jørgensen, I., Franx, M., & Kjærgaard, P. 1996, MNRAS, 280, 167 (JFK96)
Kauffmann, G., White, S. D., & Guiderdoni, B. 1993, MNRAS, 264, 201
Kewley, L. J., Geller, M. J., & Jansen, R. A. 2004, AJ, 127, 2002
Kodama, T., Yamada, T., Akiyama, M., et al. 2004, MNRAS, 350, 1005
Kormendy, J. 1977, ApJ, 217, 406
Kroupa, P. 2001, MNRAS, 322, 231
Lanzoni, B., & Ciotti, L. 2003, A&A, 404, 819
Le Borgne, J.-F., Bruzual, G., Pelló, R., et al. 2003, A&A, 402, 433
McCarthy, P. J., Le Borgne, D., Crampton, D., et al. 2004, ApJ, 614, L9
Michard, R. 1980, A&A, 91, 122
Mignoli, M., Cimatti, A., Zamorani, G., et al. 2005, A&A, in press
Pahre, M. A., Djorgovski, S. G., & de Carvalho, R. R. 1998, ApJ, 116, 1591
Pozzetti, L., Cimatti, A., Zamorani, G., et al. 2003, A&A, 402, 837
Renzini, A. 1999, in The Formation of Galactic Bulges, ed. C. M. Carollo, H. C. Ferguson, & R. F. G. Wyse (Cambridge University Press), 9
Renzini, A. 2005, in The Initial Mass Function 50 Years Later, ed. E. Corbelli, F. Palla, & H. Zinnecker (Dordrecht: Springer), 221
Renzini, A., & Ciotti, L. 1993, ApJ, 416, L49
Riciputi, A., Lanzoni, B., Bonoli, S., & Ciotti, L. 2005, A&A, in press [arXiv:astro-ph/0507664]
Saracco, P., Longhetti, M., Severgnini, P., et al. 2005, MNRAS, 357, L40
Schlegel, D. J., Finkbeiner, D. P., & Davis, M. 1998, ApJ, 500, 525
Sérsic, J. L. 1968, Atlas de galaxias australes (Cordoba, Argentina: Observatorio Astronomico)
Simard, L. 1998, in Astronomical Data Analysis Software and Systems VII, ed. R. Albrecht, R. N. Hook, & H. A. Bushouse, ASP Conf. Ser., 145, 108
Somerville, R. S., Moustakas, L. A., Mobasher, B., et al. 2004, ApJ, 600, L135
Tonry, J., & Davis, M. 1979, AJ, 84, 1511
Treu, T., Ellis, R. S., Liao, T. X., & van Dokkum, P. G. 2005a, ApJ, 622, L5
Treu, T., Ellis, R. S., Liao, T. X., et al. 2005b [arXiv:astro-ph/0503164]
van der Wel, A., Franx, M., van Dokkum, P. G., et al. 2005, submitted to ApJ [arXiv:astro-ph/0502228]
van Dokkum, P. G., & Franx, M. 2001, ApJ, 553, 90
van Dokkum, P. G., & Stanford, S. A. 2003, ApJ, 585, 78
van Dokkum, P. G., Franx, M., Kelson, D. D., & Illingworth, G. D. 1998, ApJ, 504, L17
Zoccali, M., Cassisi, S., Frogel, J. A., et al. 2000, ApJ, 530, 418

Online Material

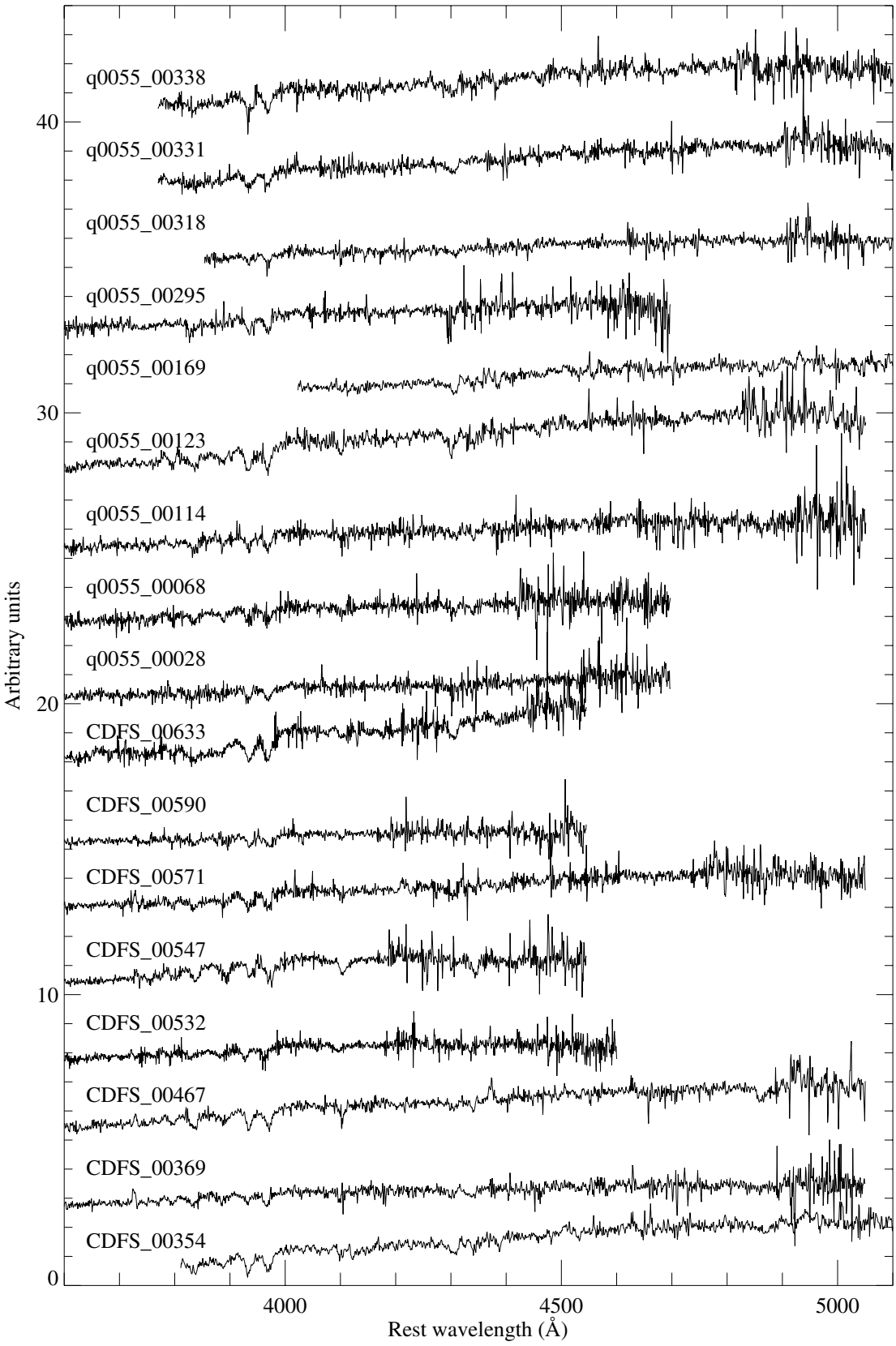

Fig. 2. The extracted spectra of all the galaxies for which we could obtain the velocity dispersion.

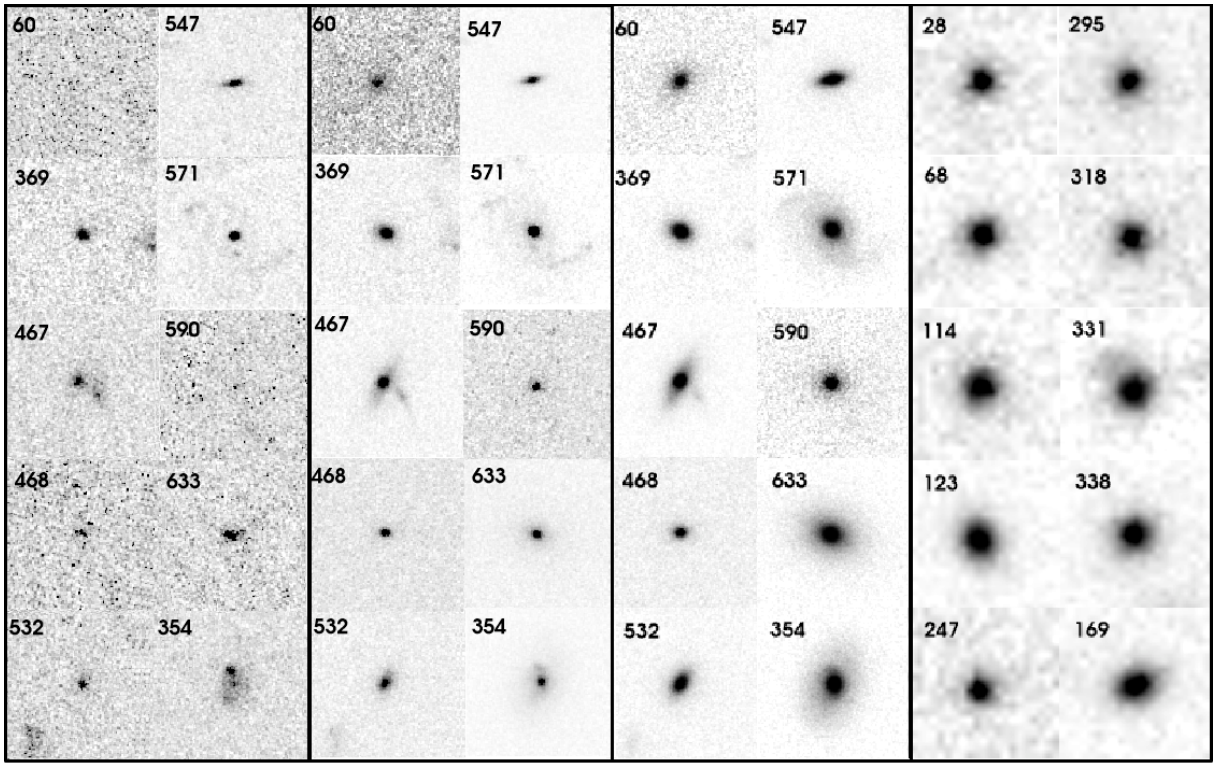

Fig. 3. Images of our galaxies from the CDFS field (3 panels on the left: HST+ACS+F435W, HST+ACS+F606W, HST+ACS+F850LP, *from left to right*) and from the 0055–269 field (*right most panel*, VLT+FORS1+Gunn z). Each box is 3×3 arcsec. The numbers in the boxes are the last 3 digits of the object's name (see Table 1).